Research Square

Preprints are preliminary reports that have not undergone peer review.
They should not be considered conclusive, used to inform clinical practice,
or referenced by the media as validated information.

# Femtosecond Laser-Activated Chitosan for Biomodification of Caries-Affected Deep Dentine: A Structural Microhardness and Laser-Induced Breakdown Spectroscopy (LIBS) Kinetic Analysis

**Safaa H. Abd-Elhakim**
Minia University
**Mahmoud G. Mahmoud**
Minia University
**Aya Eid**
Laser Institute for Research and Applications LIRA, Beni-Suef University
**Fatma Abd El-Samad**
Laser Institute for Research and Applications LIRA, Beni-Suef University
**Maha Niazy**
azhar
**Waleed M. Arafa**
Walid.ahmed@vet.bsu.edu.eg

Laser Institute for Research and Applications LIRA, Beni-Suef University
**Tarek Mohamed**
Laser Institute for Research and Applications LIRA, Beni-Suef University

**Article**

**Keywords:** Deep dentine, Femtosecond laser, Chitosan, Biomodification, Microhardness, Laser-Induced Breakdown Spectroscopy (LIBS)

**Posted Date:** November 12th, 2026

**DOI:** https://doi.org/10.21203/rs.3.rs-11428172/v1

**License:** This work is licensed under a Creative Commons Attribution 4.0 International License.
Read Full License

**Additional Declarations:** No competing interests reported.

# Femtosecond Laser-Activated Chitosan for Biomodification of Caries-Affected Deep Dentine: A Structural Microhardness and Laser-Induced Breakdown Spectroscopy (LIBS) Kinetic Analysis

**Mahmoud G. Mahmoud[1], Safaa H. Abd-Elhakim[1], Aya Eid[2], Fatma Abd El-Samad[2], Waleed M. Arafa[2], Maha Niazy[3], Tarek Mohamed[2,*]**
**[1]Faculty of Dentistry, Minia University, Minia, Egypt**
**[2]Laser Institute for Research and Applications LIRA, Beni-Suef University, Beni-Suef 62511, Egypt**
**[3]Faculty of Dental Medicine for Girls, Al- Azhar University, Cairo, Egypt**
***Corresponding author: E-mail:** Walid.ahmed@vet.bsu.edu.eg

## ABSTRACT

Deep carious dentine is highly vulnerable to acid-induced mineral loss and subsequent mechanical breakdown. This study evaluated five distinct surface conditioning approaches on artificial caries-affected human dentine (N = 40, n = 8/group): Group 1, standalone sub-ablation 750 nm femtosecond laser; Group 2, standalone sub-ablation 830 nm femtosecond laser; Group 3, combined 750 nm laser conditioning with a 2% chitosan hydrogel; Group 4, combined 830 nm laser conditioning with a 2% chitosan hydrogel; and Group 5, topical application of 2% chitosan gel alone. Experimental photoactivation was executed using a sub-ablation average power of 300 mW for 5 minutes. Surface microhardness (VHN) and raw elemental peak intensity by Laser-Induced Breakdown Spectroscopy (LIBS) tracking Calcium (317 nm) and Phosphorus (558 nm) were quantified across baseline, post-demineralization, and post-treatment intervals. Mixed-model analysis revealed highly significant main effects for both treatment stages ($p < 0.001$) and study groups ($p = 0.003$). Post-biomodification, Group 3 achieved the highest surface microhardness peak (32.34 ± 2.60 VHN), which was statistically superior to the standalone laser cohorts ($p < 0.05$). Raw LIBS intensities confirmed a parallel trend for Calcium, with Group 3 reaching optimal mineral recovery 99.45 % (56,335.85 a.u.), Conversely, standalone sub-ablation 750 nm near-infrared femtosecond laser irradiation (Group 1) achieved the highest overall post-treatment Phosphorus network retention rate of 95.44% (32,880.58 a.u.).**Conclusion:** The synergistic combination of a 750 nm near-infrared femtosecond laser operating under a non-destructive sub-ablation threshold and a concentrated 2% chitosan gel effectively biomodifies deep carious dentine by maximizing structural surface microhardness and Calcium recovery.

**Keywords:** Deep dentine; Femtosecond laser; Chitosan; Biomodification; Microhardness; Laser-Induced Breakdown Spectroscopy (LIBS).

## Introduction

Deep dentine represents a highly complex biological and structural substrate for restorative dentistry because of its elevated moisture content, high organic volume, increased tubular density and direct proximity to vital pulp tissue. These intrinsic characteristics render deep dentine exceptionally susceptible to hydrolytic degradation, endogenous enzymatic breakdown and

compromised resin-monomer infiltration. Traditional mechanical and chemical conditioning protocols often focus heavily on structural debridement while overlooking the biological dynamics of the dentine matrix. The long-term stability of restorations in deep cavities consequently remains a significant clinical concern, with hybrid layer degradation and secondary caries frequently reported. Resin elution from hydrolytically unstable polymeric hydrogels within hybrid layers may continue through nanoleakage channels during aging, rendering previously resin-infiltrated collagen matrices susceptible to attack by proteolytic enzymes[1,2]. Water-rich domains associated with the reticular mode of nanoleakage and manifested as self-propagating water trees along the adhesive–dentine junction may produce a rapid deterioration of the mechanical properties of the adhesive along this region[3,4]. Host-derived collagenolytic activity is now well documented at this interface[5,6] .To address these limitations, minimal intervention dentistry has shifted towards bioactive conditioning modalities designed to functionally modulate the dentine substrate. This philosophy is founded on early caries detection and risk assessment, remineralization of demineralized enamel and dentine, and optimal caries-preventive measures deployed across a patient's lifetime[7] ,with the general aim of reducing the invasiveness and the anxiety burden of operative treatment[8] .Among the available technologies, ultrashort-pulse laser systems, particularly femtosecond lasers, offer a highly controlled approach for inducing precise physicochemical modifications. Operating with pulse durations on the order of femtoseconds ($10^{-15}$ s), these lasers remove material in extremely thin layers with each pulse (less than 1.5 μm) while precise depth control is maintained [9] .The efficiency of laser ablation of enamel and dentine depends on wavelength, pulse duration, energy density and repetition rate, all of which can be adjusted to optimize the process for a specific tissue[9] . Reported single-shot ablation thresholds for infrared femtosecond irradiation are 1.1 ± 0.1 J/cm² for enamel and 0.6 ± 0.1 J/cm² for dentine[9], and approximately 2.0 J/cm² for enamel and 1.6 J/cm² for dentine in a 100 kHz regime operating without cooling[10]. Below these thresholds, satisfactory ablation rates with minimal thermal load and no signs of collateral damage have been documented, and intrapulpal temperature rise during irradiation has been measured to avoid irreversible pulpal damage[10]. Therefore, sub-ablation femtosecond protocols are attractive from a clinical safety standpoint, offering high precision and minimal collateral damage[11]. In dental research; near-infrared wavelengths in the 700–830 nm regions have been introduced to interact with the dental substrate. These wavelengths exhibit high spatial confinement candidates for conditioning deep dentine substrates. Clinically, laser conditioning also offers a patient-friendly alternative to conventional rotary instruments by eliminating mechanical vibration, friction and operational noise, thereby enhancing overall patient acceptance[9,11]. To capitalize on the laser-modified dentine surface, the integration of natural biopolymers has been explored [12]. Chitosan is a naturally derived linear cationic polysaccharide composed of β-linked D-glucosamine and N-acetyl-D-glucosamine, and has attracted interest because of its biocompatibility, polycationic nature and film-forming capabilities [13]. Chitosan forms a cross-link with dentine type I collagen and can block the binding site of collagenase, preventing collagen destruction, and it can also directly block collagenase in the absence of cross-linking agents[14]. Chitosan derivatives, added to

resin-based materials or adhesives, can increase the strength and stability of dentine bonds because of their biomimetic mineralization properties[14]. Its abundant hydroxyl and amino functional groups act as chelating agents capable of binding calcium ions, creating a localized, sustained microenvironment that facilitates mineral nucleation; chitosan applied to enamel surfaces can entrap calcium ions from the surrounding medium and serve as a prototype to deliver mineral ions in incipient caries[15]. Chitosan-based hydrogels also exert long-term inhibitory effects on cariogenic biofilm growth, lactic acid production and metabolic activity[16]. When applied to femtosecond laser-conditioned deep dentine, a synergistic effect is hypothesized: the laser irradiation activates the surface topography and increases permeability, allowing deeper infiltration of the biopolymer into the tubule network, while the chitosan establishes antimicrobial biofilm resistance and structural stabilization. Therefore, this study aimed to evaluate and compare the effects of five conditioning regimens on caries-affected deep dentine based on the principles of minimal intervention dentistry: standalone femtosecond laser irradiation (at 750 nm and 830 nm), 2% chitosan gel alone, and the combined application of a 2% chitosan gel with a femtosecond laser. Specifically, the study investigates changes in surface microhardness and chemical composition using Laser-Induced Breakdown Spectroscopy. The null hypothesis tested is that there is no significant difference in surface microhardness and elemental composition of caries-affected deep dentine regardless of the conditioning approach applied.

## Materials and methods

### Protocol registration and ethical approval

The Research Ethics Committee of the Faculty of Dentistry, Minia University officially approved this study protocol (Approval No. 690/2023). Experimental procedures and all the methodologies used in handling tissues were performed in line with the ethical principles, guidelines and regulations that were stipulated in the World Medical Association Declaration of Helsinki. All human donors voluntarily provided written informed consent before tooth extraction, after detailed disclosure of the research objectives and the intended use of the extracted specimens for in-vitro laboratory analysis.

### Specimen collection and power analysis

The Department of Oral and Maxillofacial Surgery of the Faculty of Dentistry, Minia University, collected 40 human molars that were extracted among people aged between 30 and 50 years, with simple carious lesions, extracted only due to therapeutic or periodontal reasons. A prospective statistical power analysis was performed to justify the use of the sample size, based on previous literature assessing dental substrate biomodification. It was calculated that the sample size of eight independent specimens per group ($n = 8$, total $N = 40$) would give a statistical power of 80% to detect meaningful differences in mechanical surface microhardness and raw elemental line intensities at a significance level of $\alpha = 0.05$. The teeth were immediately

rinsed with distilled water to eliminate the soft tissue debris and then kept in 0.1% thymol solution at 4 °C to inhibit microbial growth before being prepared in the experiment.

**Substrate Preparation**

The specimens collected were thoroughly observed under × 20 optical magnifications and radiographed with a digital intraoral X-ray sensor (Shanghai Handy Medical Equipment, Ltd., Shanghai, China) to ensure that no extensive micro-crack lines, deep root caries, previous restorative procedures, internal resorption or calcification of the pulp chamber were present. A slow-speed water-cooled diamond saw was used to mechanically remove the occlusal enamel and the surface level dentine in order to reveal flat and homogeneous deep dentine surfaces according to the existing hard tissue substrate preparation procedure described by Özcan et al.[17]. They were then embedded in blocks of self-curing acrylic resin individually using standardized cylindrical molds with a diameter of 10 mm and a height of 15 mm in a way that the prepared deep dentine surfaces could be fully exposed, level, and horizontal.

**Artificial Caries Induction**

Artificial caries-affected dentine lesions were induced by exposing the dentine blocks to a continuous 14-day regimen of chemical pH-cycling at room temperature based on the protocol adapted from Marquezan et al.[18]. Each 24-hour cycle included placing the specimens for 8 hours in a demineralizing solution with 2.2 mM $CaCl_2$ at an acidic pH of 4.8 that contained 2.2 mM $NaH_2PO_4$ and 50 mM acetic acid. After demineralization, the samples were thoroughly rinsed with deionized water and left for 16 hours in a remineralizing solution of 1.5 mM $CaCl_2$, 0.9 mM $NaH_2PO_4$, 0.15 M KCl and incubated at a neutral pH of 7.0. New solutions were made every day and precision was checked using a digital pH meter.[19]

**Experimental Groups and Surface Conditioning**

Following the 14-day chemical cycling challenge, the 40 demineralized samples were randomly allocated into five equal, parallel experimental groups (n = 8 per group) to receive their respective surface conditioning treatments directly onto the carious substrate without any prior phosphoric acid etching step:

- **Group 1 (G1):** Standalone sub-ablation femtosecond laser irradiation at a wavelength of 750 nm for 5 minutes.
- **Group 2 (G2):** Standalone sub-ablation femtosecond laser irradiation at a wavelength of 830 nm for 5 minutes.
- **Group 3 (G3):** Combined topical application of a 2% chitosan gel for 5 minutes, followed immediately by 750 nm femtosecond laser photoactivation for additional 5 minutes.
- **Group 4 (G4):** Combined topical application of a 2% chitosan gel for5 minutes, followed immediately by 830 nm femtosecond laser photoactivation for additional 5 minutes.

- **Group 5 (G5):** Topical application of 2% chitosan gel alone left undisturbed on the matrix surface for 5 minutes.

**Preparation of Chitosan Hydrogel**

The biopolymer agent used was a 2% physical chitosan hydrogel prepared by dissolving medium molecular weight chitosan (poly [D-glucosamine], ~150 kilodaltons (kDa), degree of deacetylation >85%), in a 1% (v/v) aqueous solution of acetic acid, which gave a standardized gel pH of 5.5. The protocols that were followed in the treatments were executed in stringently controlled lab conditions. No secondary ion-containing storage medium or saliva bath was used after treatment, so the measured elemental or structural changes arose solely from the immediate interactions of the conditioning protocols.

**Surface Microhardness Assessment**

Surface microhardness of the exposed deep dentine substrates was measured at three intervals of the experiment namely baseline, after demineralization and after the applied conditioning treatments. The testing was performed using a digital microhardness tester (TUKON 1102; Wilson Hardness, Buehler ITW, Aachen, Germany) with a calibrated diamond Vickers indenter. A series of three different indentations were done on each specimen at a controlled subsurface distance of 30 μm from the outer operational margin with a clear inter-indentation distance of 100 μm between the indentations to prevent localized stress-field effects and inter-measurement contamination. A standardized load of 50 gf (0.49 N) was used and applied smoothly without causing impact and held at rest with a dwell time of 15 seconds to provide accurate indentation and accommodate the viscoelastic nature of dentine.[20] After the load was removed, the geometric impression was brought into optical focus using high-magnification eyepieces. The two perpendicular diagonals of the impression were measured to the nearest 0.1 μm using the integrated digital micrometer system. The average diagonal length then was used to automatically calculate Vickers Microhardness Number (VHN) using the standard mathematical equation.

$$\mathbf{VHN = (1854.4 \times L) / d^2}$$

Where (L) represents the applied indentation load in grams-force (gf) and (d) denotes the computed arithmetic average of the two indentation diagonal lengths in micrometers (μm). The final surface microhardness value assigned to each specimen at each testing phase was established as the mathematical mean derived from its three individual indentation readings.

**Elemental Composition Analysis via Laser-Induced Breakdown Spectroscopy (LIBS)**

Deep dentine samples were compositionally tracked using Laser-Induced Breakdown Spectroscopy (LIBS) at baseline, after demineralization and after treatment. A high-power, Q-

switched Nd:YAG laser system (Quanta-Ray PRO 350; Spectra-Physics, Santa Clara, CA, USA) which used the second harmonic wavelength of 532 nm with a fixed pulse duration of 10 ns and a repetition rate of 10 Hz was used to produce localized plasma on the substrate. Each specimen was placed on a three-axis micro-translation stage, which was controlled by a computer to obtain accurate micro-positioning, preventing overlap between spots in a reading. The laser beam (nanosecond) was directed to the surface of the dentine to produce a standardized spot diameter of 100 μm with optimized pulse energy of 10 mJ.

A dedicated multi-site mapping protocol was used to prevent the destructive laser ablation during LIBS sampling from confounding subsequent measurements. Three separate measurements of the dentine surface were captured as single-shots at three different lateral locations within an experimental interval with a minimum of 1.0 mm between sites. A new surface area would be ablated with each single laser shot, and the craters of the plasma in the past would not affect the elemental readings of the next. The average of these three different acquisitions was determined mathematically to determine the final elemental value at any given stage.

The resultant plasma optical emission was collected by a high-collection efficiency VIS collimating lens (74-VIS; Ocean Insight, Orlando, FL, USA) and focused into an optical fiber assembly (QP600-2-SR). The emission signals were then fed into a high resolution digital spectrometer (FLAME-S-XR1; Ocean Insight, Orlando, FL, USA). Spectral data was collected at an optimized delay time of 1 μs and integration time of 10 μs to maximize the signal-to-background ratio. The spectral recording processes were performed at normal atmospheric pressure. Quantitative monitoring used the Calcium (Ca I) line at 317 nm and the Phosphorus (P I) line at 558 nm, corresponding to the core atomic emission peaks used to characterize structural dentine.[21]

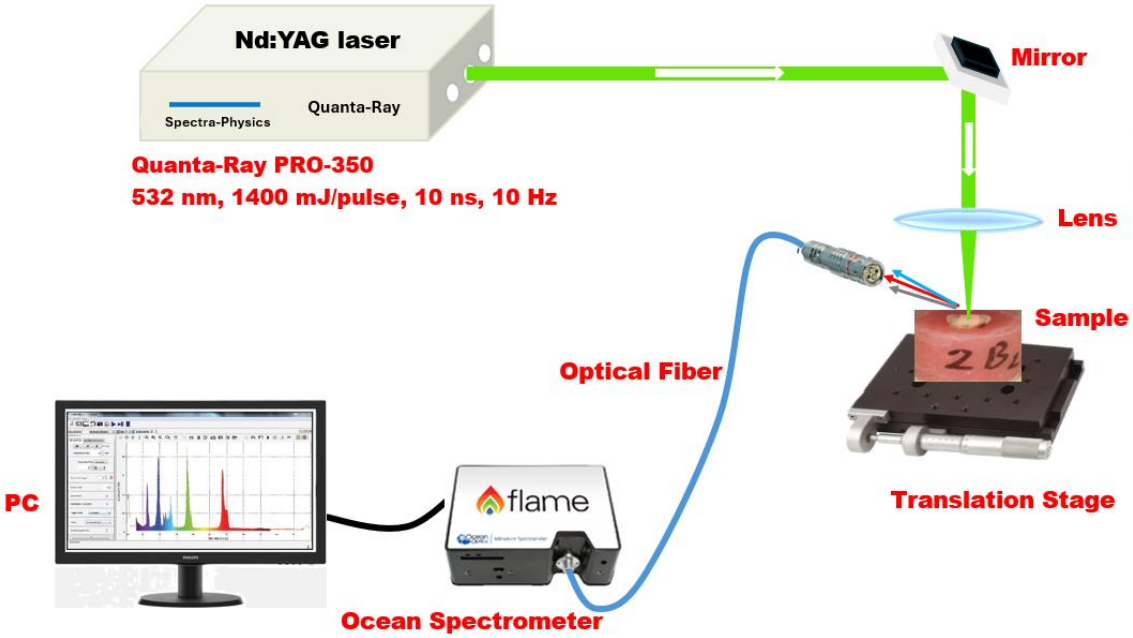



**Figure 1:** Schematic configuration of the high-power, Q-switched Nd: YAG laser-induced breakdown spectroscopy (LIBS) system

**Protocol of Samples modification by Femtosecond Laser:**

Therapeutic substrate conditioning was performed using high-precision femtosecond laser system (INSPIRE HF 100; Spectra-Physics, Santa Clara, CA, USA) pumped by mode-locked (Ti:Sapphire) laser source (Mai-Tai HP; Spectra-Physics), tuned to a near-infrared wavelength 690–1040 nm with a baseline average output power of 1.5–2.9 W, a fixed pulse repetition rate of 80 MHz, and an ultrashort pulse duration of 100 fs. To achieve the desired treatment effects on the targeted groups (G1, G2, G3, and G4), the irradiation was performed at two targeted treatment wavelengths, namely, 750 nm and 830 nm. The working average output power delivered to the dentine surface was accurately attenuated and set to 300 mW using a calibrated optical power meter (Newport 843-R; RK Tech Ltd., Budapest, Hungary).

The laser beam path was guided through a sequence of very reflective dielectric mirrors, and through a manual variable attenuator to tightly regulate delivery of energy. This was done by focusing the beam perpendicular to the exposed flat deep dentine surface at a constant, standardized probe-to-tissue distance of 10 mm in the absence of active water cooling under dry environmental conditions to avoid gel dilution. The focal spot profile had a standardized diameter of 100 μm, which provided a spot beam area of $7.85 \times 10^{-5}$ cm² and the operating average power density of 3.82 kW/cm². The estimated value of the single-pulse energy was 3.75 nJ, such that the maximal intensities were kept strictly in a sub-ablation regime to induce photo-physical matrix conditioning rather than thermal or mechanical tissue ablation.[9, 10]

The total exposure time was fixed at 5 minutes per specimen. For the combined treatment groups (G3 and G4), the 2% chitosan gel was evenly applied as a 1.0-mm uniform layer across the demineralized dentine surface immediately prior to the 5-minute laser irradiation.

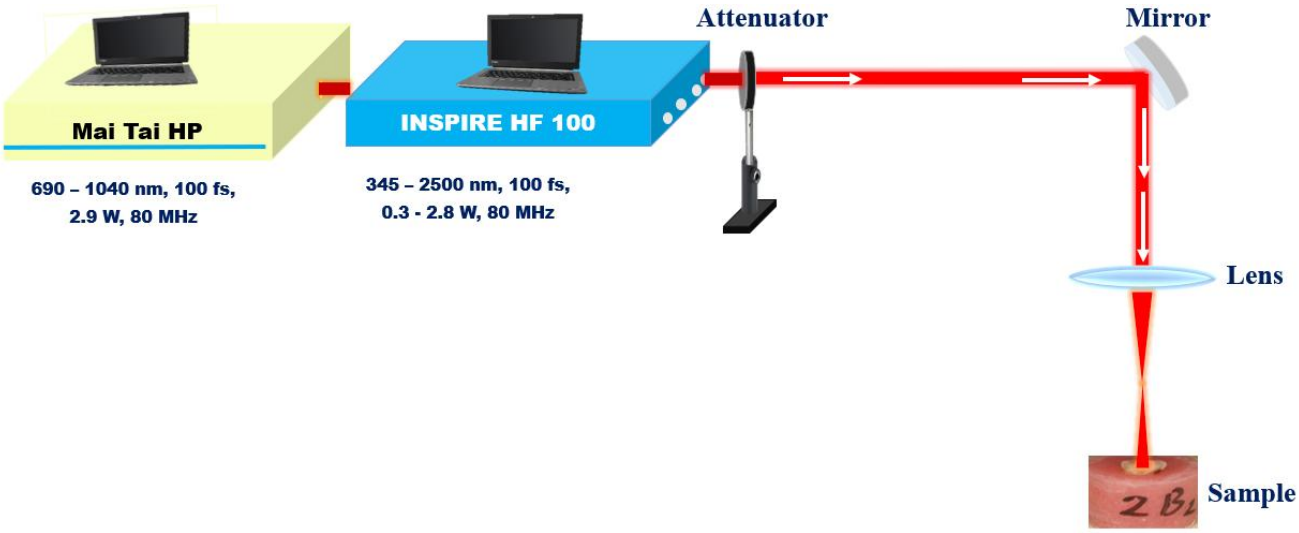



**Figure 2**: Schematic setup for the femtosecond laser photoactivation of carious dentine sample.

**Statistical analysis**

Normality was assessed using the Shapiro-Wilk test together with inspection of model residuals. Because hardness and elemental profiles were measured repeatedly on the same specimens at baseline, after demineralization, and after remineralization/biomodification, the primary analysis used a two-way mixed repeated-measures ANOVA, with study group (Groups 1–5) as the between-subject factor and treatment stage as the within-subject factor. Data were summarized as mean and standard deviation (SD).

The model evaluated the main effects of study group and treatment stage and the group × treatment-stage interaction. Within each group, planned pairwise comparisons between treatment stages were performed using paired samples t-tests. Comparisons among the five independent groups at each treatment stage were performed using one-way ANOVA followed, when significant, by Tukey's honestly significant difference (HSD) post-hoc test. Statistical significance was set a priori at $p \leq 0.05$. Analyses were performed using IBM SPSS Statistics, version 25 (IBM Corp., Armonk, NY, USA).

**Results:**

**1- Microhardness**

- **Baseline Control Stage:** One-way ANOVA confirmed no statistically significant differences in structural hardness parameters among the five randomized groups ($p = 0.112$). Mean

microhardness ranged from a minimum of 54.19 ± 3.70 VHN in Group 1 to a peak of 61.93 ± 6.03 VHN in Group 4.

- **Post-Demineralization Carious Stage:** Hardness metrics varied significantly across the independent cohorts (one-way ANOVA, p = 0.001). Tukey's HSD post-hoc evaluation revealed a significantly harder carious surface in Group 5 (31.60 ± 2.83 VHN) compared to Group 1 (24.46 ± 3.00 VHN, *p = 0.001*), Group 2 (25.67 ± 3.20 VHN, *p = 0.009*), and Group 4 (26.27 ± 2.54 VHN, *p = 0.023*).
- **Post-Treatment Biomodification Stage:** Mechanical properties post-conditioning differed significantly among the five study groups (one-way ANOVA, *p = 0.002*). Tukey's post-hoc tests confirmed that Group 3 achieved the absolute highest post-treatment surface stiffness peak (32.34 ± 2.60 VHN), which was statistically superior to standalone Group 1 (27.52 ± 2.67 VHN, *p = 0.007*) and standalone Group 2 (28.20 ± 1.89 VHN, *p = 0.027*). Additionally, Group 5 (31.79 ± 2.88 VHN) retained significantly higher microhardness properties than Group 1 (*p = 0.021*). Figure 3 and Table 1 show the changes in five study groups

**Table 1:** Mean ± SD [SEM] surface microhardness values (VHN) for the five study groups across experimental stages.

| **Experimental Group (n = 8)** | **Baseline Control Stage (VHN)** | **Post-Demineralization Carious Stage (VHN)** | **Post-Treatment Biomodification Stage (VHN)** | ***p*-value (Within-Group)** |
|---|---|---|---|---|
| **Group 1** (Standalone 750 nm) | 54.19 ± 3.70 | 24.46 ± 3.00 [a] | 27.52 ± 2.67 [± 0.94] [x] | <0.001* |
| **Group 2** (Standalone 830 nm) | 58.63 ± 5.64 | 25.67 ± 3.20 [± 1.13] [a] | 28.20 ± 1.89 [± 0.67] [x,y] | <0.001* |
| **Group 3** (750 nm + Chitosan) | 57.73 ± 6.65 | 29.23 ± 4.67 [± 1.65] [*a,b*] | 32.34 ± 2.60 [± 0.92] [y] | <0.001* |
| **Group 4** (830 nm + Chitosan) | 61.93 ± 6.03 | 26.27 ± 2.54 [± 0.90] [a] | 29.53 ± 3.01 [± 1.06] [*x,y*] | <0.001* |
| **Group 5** (Standalone Chitosan) | 60.07 ± 6.20 [± 2.19] | 31.60 ± 2.83 [± 1.00] [b] | 31.79 ± 2.88 [± 1.02] [y] | <0.001* |

| | | | | |
|---|---|---|---|---|
| ***p*-value (Between-Group)** | 0.112 (ns) | 0.001* | 0.002* | |

*Note:* Values are expressed as Mean ± Standard Deviation [± Standard Error of the Mean (SEM)]. *Statistically significant at $p \leq 0.05$; *ns*: non-significant ($p > 0.05$) via Mixed Two-Way Repeated-Measures ANOVA. Different superscript letters within the same vertical column (*a*, *b* for demineralization; *x*, *y* for post-treatment) indicate statistically significant differences between groups at that specific stage based on Tukey's HSD post-hoc testing ($p \leq 0.05$).

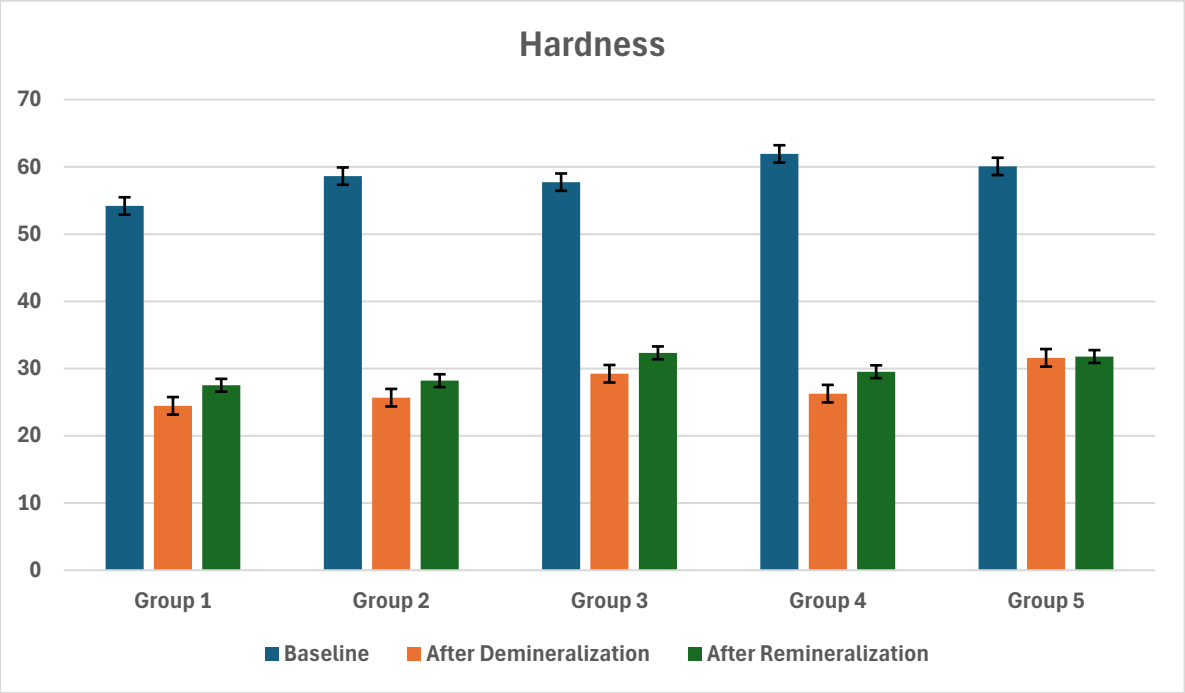



**Figure 3:** Clustered surface microhardness distributions (VHN) for the five study groups at each experimental checkpoint.

## 2- Laser-Induced Breakdown Spectroscopy (LIBS)

### Baseline elemental characterization of intact dentin

Laser-induced breakdown spectroscopy (LIBS) showed a typical emission profile of a mineral in sound dentin. Several emission lines were identifiable throughout the wavelength range studied, with calcium (Ca) and phosphorus (P) being the most prevalent signals of mineral nature. Calcium-related emission lines were prominent at approximately 300–460 nm (Figure 6A), while a strong phosphorus signal appeared near 558 nm (Figure 6B). There were also additional signals which could be attributed to Na, Mg, O, Fe and other trace elements. The positions of the principal peaks were consistent across the baseline spectra, but variations were primarily associated with the intensity of the emissions, as shown in figure 4.

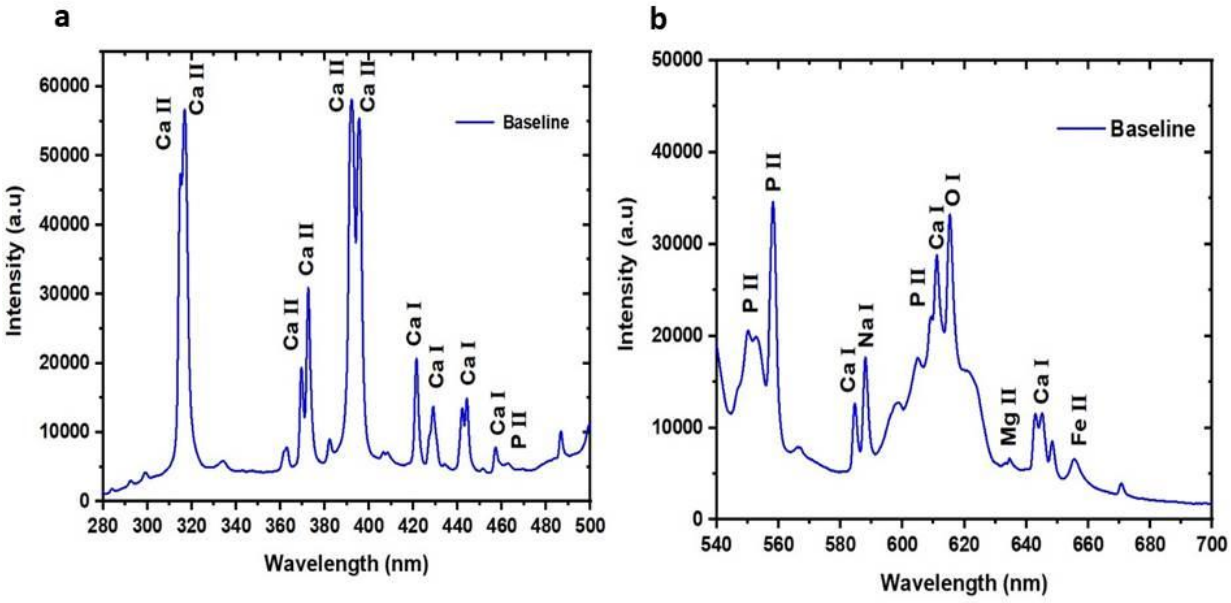



**Figure 4:** Representative baseline Laser-Induced Breakdown Spectroscopy (LIBS) emission profiles recorded within intact human dentine, showcasing (a) the principal Calcium (Ca I) peak structures across the 300–460 nm spectral window and (b) the prominent Phosphorus (P II) atomic line signal targeted at approximately 558 nm.

**Effect of demineralization on Ca and P signals:**

Demineralization resulted in a steady decrease in the major mineral-related LIBS signals. It was observed that the decrease was clear at Ca at a wavelength of about 317 nm and P at a wavelength of about 558 nm. Across the three baseline groups, Ca intensity decreased from 56,520.94, 56,042.72 and 56,648.76 a.u. to 43,883.75, 41,104.84 and 44,343.65 a.u., respectively. P intensity similarly decreased from 34,451.04, 32,640.06 and 35,639.50 a.u. to 26,910.01, 21,788.34 and 22,764.57 a.u., respectively. The findings show that there is a marked loss of Ca- and P-related spectral intensity after demineralization as demonstrated in table 2.

**Table 2:** Baseline and post-demineralization raw elemental line intensities for Calcium (Ca I at 317 nm) and Phosphorus (P I at 558 nm) across the primary evaluation tracking groups.

| Element | Group | Baseline (a.u.) | After demineralization | Direction of |
|---|---|---|---|---|

| | | | (a.u.) | change |
|---|---|---|---|---|
| Ca | 1 | 56,520.94 | 43,883.75 | Decrease |
| Ca | 2 | 56,042.72 | 41,104.84 | Decrease |
| Ca | 3 | 56,648.76 | 44,343.65 | Decrease |
| P | 1 | 34,451.04 | 26,910.01 | Decrease |
| P | 2 | 32,640.06 | 21,788.34 | Decrease |
| P | 3 | 35,639.50 | 22,764.57 | Decrease |

**Note:** Data represent raw mean atomic emission line intensities quantified in arbitrary units (a.u.). Statistical significance was verified utilizing a two-way mixed repeated-measures ANOVA followed by Tukey's post-hoc adjustments ($p \leq 0.05$).

**Ca response to 750 nm laser, chitosan and their combination to biomodification:**
At the Calcium emission wavelength of approximately 317 nm, all post-demineralization treatment conditions showed statistically significant recovery of the Calcium-associated signal ($p = 0.002$). Standalone 2% chitosan gel produced an intensity of 50,146.77 a.u., while standalone 750 nm laser irradiation produced 54,231.56 a.u. The 750 nm laser plus chitosan combination (Group 3) produced the absolute highest value within this treatment set (56,335.85 a.u.), which closely approached the baseline Calcium range and was statistically superior to standalone 750 nm laser conditioning ($p = 0.007$). (Fig.5)

**Table 3:** Quantitative post-treatment Calcium (Ca I at 317 nm) line intensity distributions following standalone 750 nm laser, standalone chitosan hydrogel, and combined laser–chitosan treatment.

| Condition | Ca intensity at 317 nm (a.u.) | Percentage |
|---|---|---|
| Demineralization | 41,104.84 – 44,343.65 | 21.72% - 26.65% drop from its specific baseline |
| Chitosan | 50,146.77 | 88.8% |
| 750 nm | 54,231.56 | 95.9 % |
| 750 nm + chitosan | 56,335.85 | 99.45 % |
| Baseline | 56,042.72–56,648.76 | 100 % |

**Note:** Data layout, unit parameters (a.u.), and statistical reporting protocols are identical to those described in Table 2.

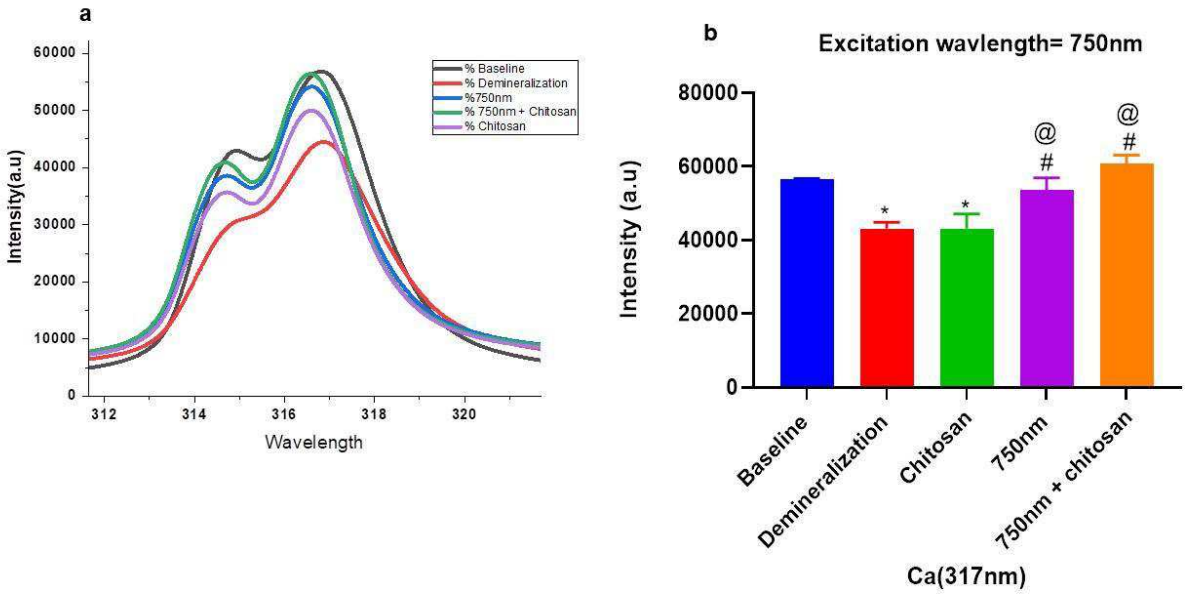



**Figure 5:** Effect of 750 nm irradiation, chitosan, and their combination (chitosan + 750 nm) on calcium (Ca) recovery. (a) LIBS spectra of Ca. (b) Statistical analysis of Ca recovery. Statistical significance was determined using one-way ANOVA followed by Tukey's post hoc test. $P < 0.05$ was considered statistically significant. *Significantly different from baseline; # significantly different from chitosan; @ significantly different from 750 nm irradiation alone.

**Ca response to 830 nm laser, chitosan and their combination to biomodification:**

The 830 nm treatment set showed a parallel recovery pattern. Calcium intensity following standalone 830 nm irradiation was 50,765.68 a.u., whereas the combined 830 nm plus chitosan protocol produced a 56,088.28 a.u. The combination therefore significantly approached the baseline Ca range, exceeding the Ca intensity observed with either standalone 830 nm irradiation or standalone chitosan ($p < 0.05$). Across all post-demineralization treatments, the definitive numerical order of statistical recovery was 750 nm + chitosan > 830 nm + chitosan > 750 nm > 830 nm > chitosan. (Fig.6)

**Table 4:** Quantitative post-treatment Calcium (Ca I at 317 nm) line intensity distributions following standalone 830 nm laser, standalone chitosan hydrogel, and combined laser–chitosan treatment.

| Condition | Ca intensity at 317 nm (a.u.) | Percentage |
|---|---|---|
| Chitosan | 50,146.77 | 88.85% |
| 830 nm | 50,765.68 | 90.58% |
| 830 nm + chitosan | 56,088.28 | 99.38% |
| Baseline | 56,042.72–56,648.76 | 100 % |

**Note:** Data layout, unit parameters (a.u.), and statistical reporting protocols are identical to those described in Table 2.

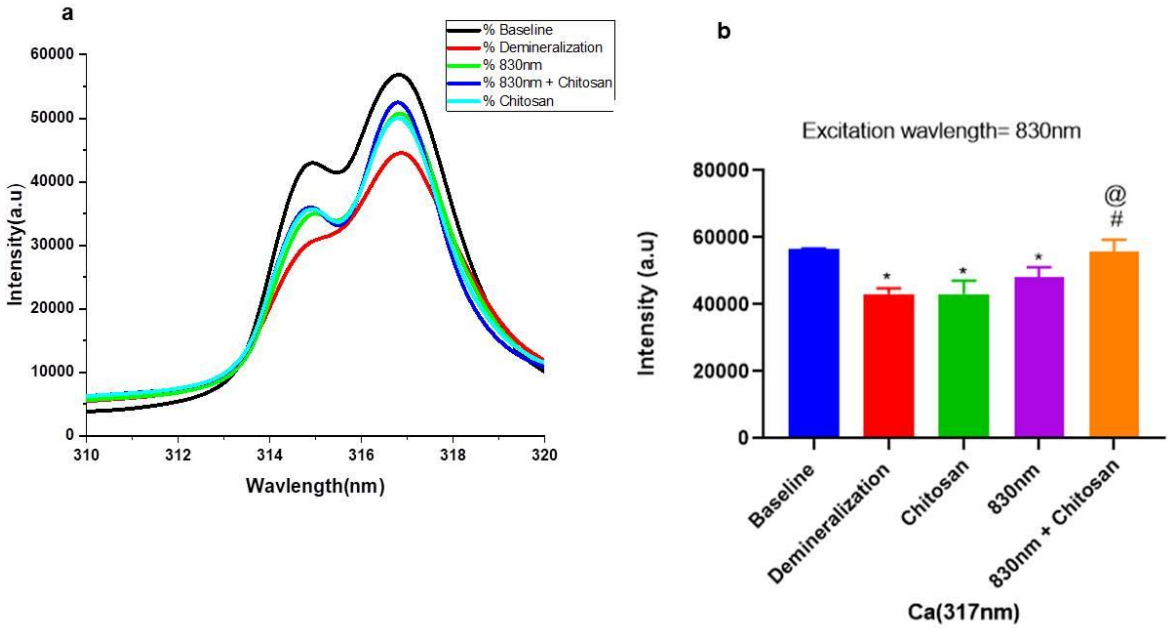



**Figure 6:** Quantitative tracking of Calcium (317 nm) recovery under 830 nm laser protocols. (a) Representative LIBS emission spectra. (b) Relative mean intensities (a.u. ± SD). Statistical comparisons performed using one-way ANOVA and Tukey's HSD test *($p \leq 0.05$). Significant differences from baseline (*), standalone chitosan (#), and standalone 830 nm laser (@) are indicated*

**Phosphorus (P) response after remineralization:**

Two-way mixed repeated-measures ANOVA at the Phosphorus emission wavelength at about 558 nm showed that the changes in the sequential phases of the experiment were highly significant ($F(2,70) = 712.45, p < 0.001$). A drastic structural decline in the Phosphorus line intensities of all groups was induced by the chemical pH-cycling challenge down to a compressed demineralized floor of between 21,788.34 a.u. and 26,910.01 a.u. and then decoupled elemental pathways were registered by the implementation of the specified surface conditioning protocols. The absolute highest post-treatment Phosphorus signal expansion was 32,880.58 a.u. with Standalone 750 nm near-infrared femtosecond laser irradiation (Group 1), indicating an optimal network recovery with a net retention rate of 95.44% that is nearly the same as with its native intact baseline parameters. On the other hand, photo-physical conditioning with a laser of 750 nm and 2% chitosan gel (Group 3), resulted in a recovery peak of 31,721.84 a.u. (89.01% retention). Conversely, the isolated 2% chitosan biopolymer cohort (Group 5) had a post-treatment signal stabilization of 27,110.45 a.u. (79.41% retention), which was consistent with the graphic distributions. Moreover, the joint 830 nm laser-chitosan application (Group 4) led to the relative inhibition of the mineral matrix, which decreased to 26,829.37 a.u. ($p = 0.009$). One-way ANOVA followed by Tukey's post-hoc testing confirmed that standalone sub-ablation 750 nm conditioning was statistically better than all the 830 nm cohorts and the standalone biopolymer matrix ($p < 0.05$).

**Table 5:** Quantitative raw elemental atomic emission line intensities for Phosphorus (P I) tracked via LIBS.

| Experimental Group | Baseline (a.u.) | After Demineralization (a.u.) | Post-Treatment Biomodification (a.u.) | Net Retention Rate (%) |
|---|---|---|---|---|
| **Group 1** (Standalone 750 nm) | 34,451.04 | 26,910.01 | 32,880.58 | 95.44% |
| **Group 2** (Standalone 830 nm) | 32,640.06 | 21,788.34 | 25,933.10 | 79.45% |
| **Group 3** (750 nm + Chitosan) | 35,639.50 | 22,764.57 | 31,721.84 | 89.01% |
| **Group 4** (830 nm + Chitosan) | 33,950.80 | 23,110.15 | 26,829.37 | 79.02% |
| **Group 5** (Standalone Chitosan) | 34,140.20 | 24,250.60 | 27,110.45 | 79.41% |

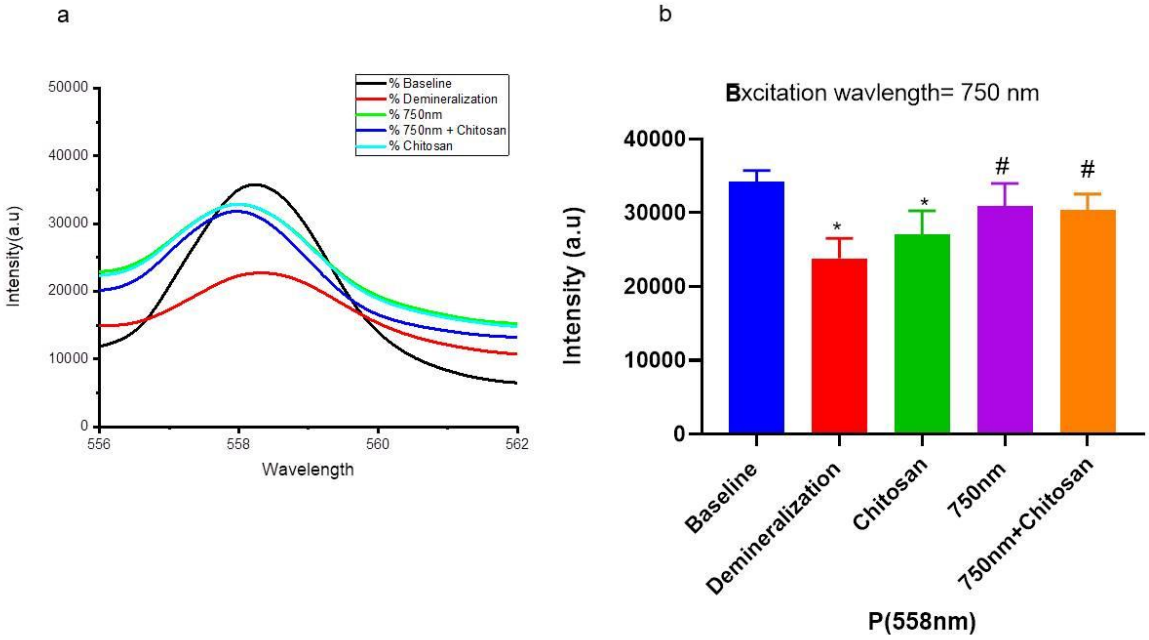


**Figure 7:** Quantitative spectral investigations of Phosphorus recovery under 750 nm laser protocols. (a) LIBS spectra of P I at 558 nm. (b) Statistical bar chart of P intensity in arbitrary units (a.u.). Significance was determined using ANOVA with Tukey's post-hoc test *($p \leq 0.05$).* **Significantly different from baseline control; # significantly different from chitosan alone.*

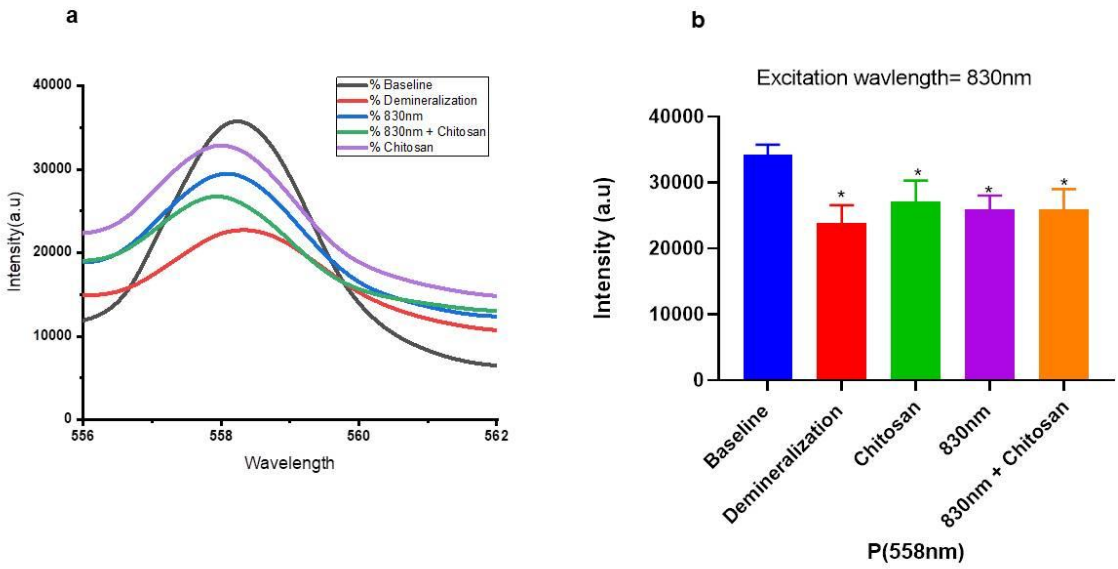



**Figure 8:** Quantitative spectral investigations of Phosphorus recovery under 830 nm laser protocols. (a) LIBS spectra of P I at 558 nm. (b) Statistical bar chart of P intensity in arbitrary units (a.u.). Significance was determined using ANOVA with Tukey's post-hoc test *($p \leq 0.05$).* **Significantly different from baseline control parameters.*

**Overall LIBS findings**

Overall, demineralization significantly reduced both Ca- and P-associated LIBS intensities ($p < 0.001$). Remineralization/biomodification produced a substantial recovery of both elemental signals, but the treatment patterns differed completely by element. Calcium recovery was greatest numerically and statistically with the laser–chitosan combinations, particularly 750 nm plus chitosan (Group 3) ($p = 0.002$), whereas Phosphorus recovery did not show the same combination-dependent pattern, favoring standalone conditioning instead. Accordingly, the statistical analysis mandates that calcium and phosphorus be interpreted as separate, decoupled kinetic tracks rather than assuming both mineral-associated signals respond identically to the tested interventions.

**DISCUSSION**

According to the statistical results of this study, the null hypothesis according to which no significant differences in the surface microhardness and elemental composition between the conditioning approaches should appear was rejected. The statistical analysis showed that the variations in both mechanical performance and elemental tracking across the evaluated groups and treatment stages were highly significant.

The study results showing that the 14-day chemical pH-cycling model triggered a severe collapse in surface structural microhardness, with values decreased sharply from an intact range of ~54–61 VHN down to a softened floor of 24.46 ± 3.00 VHN [18]. This mechanical degradation directly reflects the rapid dissolution of the hydroxyapatite crystal lattice within the inorganic matrix scaffold under acid attack [22]. Because deep dentine has a high organic volume, elevated moisture content, and high tubular density, it provides a low-resistance pathway for rapid hydrogen acid influx and subsequent mineral efflux [23]. This high structural porosity allows sub-surface mineral leaching to progress rapidly while leaving the underlying collagen scaffold completely unprotected and vulnerable to host-derived enzymatic degradation over time [2,24].

After advanced surface conditioning, the combined 750 nm near-infrared femtosecond laser and 2% chitosan gel protocol (G 3) achieved the absolute highest post-treatment surface stiffness peak of 32.34 ± 2.60 VHN [9]. This mechanical recovery was statistically superior to both standalone 750 nm laser conditioning (Group 1, 27.52 ± 2.67 VHN; $p = 0.007$) and standalone 830 nm laser conditioning (Group 2, 28.20 ± 1.89 VHN; $p = 0.027$) [25]. This synergistic mechanical recovery can be attributed to two parallel pathways. First, the sub-ablation laser energy safely increases surface free energy and permeability without causing collateral thermal matrix collapse or microscopic cracks [9,10]. Operating strictly below the single-shot ablation thresholds of dentine avoid adverse intrapulpal temperature rises while safely unroofing blocked tubules to allow deeper infiltration of the biopolymer hydrogel [11].

Second, the abundant protonated amino groups ($NH_3^+$) within the high-viscosity 2% physical hydrogel establish a powerful electrostatic attraction to incoming minerals, effectively cross-linking the exposed collagen fibrils and buffering the deep calcified substrate [14]. This outcome directly supports the zymographic findings reported by Baena et al., proving that viscous linear biopolymers successfully reinforce compromised dental matrices, limit hydrolytic breakdown, and aggressively inhibit host-derived endogenous matrix metalloproteinases (MMPs) [24].

Caries-affected deep dentine exhibited a pronounced decrease in raw Ca and P emission intensities, confirming substantial mineral dissolution under the acid challenge [25] . Concurrently, the physical collapse in surface microhardness directly correlated with this severe mineral loss, dropping significantly across all experimental cohorts. The combined application of a sub-ablation near-infrared femtosecond laser and a 2% chitosan gel induced significant chemical alterations in the demineralized substrate, shifting the tracked LIBS emission signals towards a favorable mineral trajectory close to intact baseline parameters. This multi-phase evaluation protocol effectively tracks immediate tissue dynamics, providing an appropriate baseline for testing advanced therapeutic conditioning modalities [26]

The selection of LIBS for this study based on its emerging status as a powerful analytical technique for elemental mapping in biological calcified tissues, Unlike conventional methods that require aggressive sample preparation, which may alter surface chemistry, LIBS offers real-time, minimally destructive multi-elemental analysis with minimal preparation[27], Simultaneous exploitation of spectral information from more than one element, in the form of line intensity ratios combined with pattern recognition, has been shown to be a sensitive means of distinguishing healthy from carious dental tissues[26]. and atomic and ionic emission lines belonging to P, Ca, Mg, Zn, K, Sr, C, Na, H and O have been used with multivariate discriminant analysis to discriminate and predict unknown tooth tissues[27] This capability is particularly valuable in cariology research, where tracking dynamic mineral changes during demineralization–remineralization processes within identical specimens is crucial, and the LIBS method has proved reliable for providing data on the elemental composition of root canal dentine [28], Threshold ablation energy densities differ markedly between tissues, the computed threshold for calcium ablation being 0.38 J/cm² in dentine and 1.41 J/cm² in enamel; because dentine contains pores, voids and bubbles that facilitate ablation at low energy density while enamel presents a closely packed structure requiring higher energy densities[29] This tissue-dependent behavior supports the use of carefully controlled sampling energies[30].

The LIBS spectra acquired in this study gave clear emission peaks of calcium (Ca I at 317 nm) and phosphorus (P I at 558 nm) which is in line with the reported emission lines of the hydroxyapatite reference matrices under the optimal conditions of the laser wavelength, defocus, pulse energy, and gate delay[30]. Quantitative analysis focused on these peaks because calcium and phosphorus are the main constituents of hydroxyapatite, the fundamental mineral phase in dentine. In order to remove any measurement artifacts associated with the micro-destructive character of individual laser shots, a special multi-site mapping protocol, in which the spatial separation between locations was 1.0-mm, was performed, such that the cumulative effect of prior plasma craters did not affect the subsequent measurements [31,32] .This sequence avoids localized signal distortion and maintains consistent stoichiometry reporting at every experimental interval[33].

The current results revealed that there was a major reduction in the intensity of calcium and phosphorus under the demineralization protocol ($p < 0.001$). Quantitative analysis showed that calcium signals fell from the intact baseline range of 56,042.72–56,648.76 a.u. to 41,104.84–44,343.65 a.u. after demineralization, Phosphorus signals decreased by 33.6% from baseline to a range of 21,788.34–26,910.01 a.u. This rapid mineral depletion directly caused a marked loss of surface microhardness across all laser groups ($F(2,70) = 894.785, p < 0.001$), reaching 24.46 ± 3.00 VHN in Group 1 and 29.23 ± 4.67 VHN in Group 3. This correlated mineral and mechanical loss validates the usefulness of the pH-cycling model in the formation of caries-like lesions, which is similar to the subsurface dissolution caused by alternating demineralizing and remineralizing solutions in this model[25]

The simultaneous depletion of both elements supports the established understanding that caries progression involves dissolution of the hydroxyapatite crystal lattice rather than selective

leaching of a single element. This can be attributed to the high organic and water content present in deep dentine, which facilitates the rapid influx of acids and the subsequent efflux of structural minerals, causing subsurface demineralization. The retention of bound and free water within the porous organic matrix, together with incomplete resin infiltration, is recognized as a principal route by which the dentine substrate becomes susceptible to hydrolytic and enzymatic deterioration [22,23]

The combination of a femtosecond laser and chitosan achieved promising results regarding substrate biomodification and mechanical reinforcement. Across all testing, the combined formulation groups were effective in maximizing surface microhardness compared with standalone laser treatments. This was highlighted by Group 3 (750 nm + 2% chitosan) achieving the highest post-treatment surface stiffness peak of 32.34 ± 2.60 VHN, which was statistically superior to standalone 750 nm laser conditioning (Group 1, 27.52 ± 2.67 VHN; $p = 0.007$) and standalone 830 nm laser conditioning (Group 2, 28.20 ± 1.89 VHN; $p = 0.027$). This outcome is consistent with the recognized clinical advantage of femtosecond systems, namely high precision and minimal collateral damage, achieved because material removal proceeds in very thin layers under precise depth control[11] Sub-ablation operation below the reported single-shot thresholds, without active water cooling, has also been shown to avoid collateral thermal damage and measurable intrapulpal temperature rises, which is essential when conditioning a substrate in direct proximity to the pulp[10,34].

Nevertheless, the greatest discovery of this work is the differing trends in remineralization of calcium and phosphorus in various treatment groups, which questions the traditional belief of very strong linkage of mineral re-precipitation. The combined laser-chitosan formulations were found to maximize calcium line intensity recovery and structural microhardness whereas the biopolymer group alone showed independent phosphorus retention kinetics suggesting that varied conditioning modalities change the mineral matrix via varied biochemical pathways. This observation is in contrast with classical dental remineralization concepts which presume that the precipitation of minerals is always in a fixed, perfectly coupled stoichiometric Ca:P ratio. Native enamel and enamel-like biomimetic layers reconstituted under polysaccharide hydrogels exhibit a Ca/P ratio of about 1.64[35], which is close yet not equal to the stoichiometric value of hydroxyapatite and calcium phosphate systems are known to proceed via an amorphous precursor phase that forms early on and then converts to apatite [36], such that non-stoichiometric intermediate states are kinetically accessible. The current information suggests that the two elements can have their surface kinetic rates changed independently through the use of advanced biomodification.

The present results support the role of chitosan as an effective remineralizing and stabilizing agent. Group 5, treated with standalone 2% chitosan gel, demonstrated protective behavior, maintaining high microhardness properties (31.60 ± 2.83 VHN) immediately post-demineralization and stabilizing at a post-treatment value of 31.79 ± 2.88 VHN, while achieving a post-treatment phosphorus intensity of 27,110.45 a.u. (79.41% retention relative to baseline). This can be attributed to chitosan's polycationic nature and chelating properties[36]. Under acidic

challenges, the protonated amino groups in chitosan exert a strong electrostatic attraction on negatively charged phosphate ions, while its hydroxyl functional groups simultaneously coordinate calcium ions, effectively acting as a template for hydroxyapatite nucleation. Chitosan applied to mineralized surfaces can entrap calcium ions from the surrounding medium and, combined with self-assembled peptides, deliver mineral ions into incipient lesions[36]. Hydrogel systems based on chitosan promote the remineralization of early enamel lesions, as indicated by surface microhardness, polarized light microscopy and transverse microradiography[37]. Structural shielding of this kind directly retards mechanical softening; chitosan forms a cross-link with dentine type I collagen, protects collagen, blocks the binding site of collagenase and can directly block collagenase even without cross-linking agents[14]. Zymographic analysis has shown a reduction in matrix metalloproteinase activity in mineralized and demineralized dentine powder after chitosan application[24]

It is worth noting, however, that the same study reporting reduced MMP activity found that a 0.1% chitosan solution used as an additional primer did not increase the longevity of resin–dentine bonds[24]. The discrepancy between that outcome and the mechanical protection observed here is best explained by the formulation used in the present work: a 2% physical chitosan hydrogel of medium molecular weight with a >85% degree of deacetylation, applied as a 1.0-mm layer. Higher-viscosity physical gels provide greater tubular occlusion, viscoelastic damping and matrix reinforcement than the dilute, more fluid solutions customarily used in earlier bonding studies. The durability of the resin–dentine interface is known to depend on preservation of the collagen matrix and on limiting hydrolytic and enzymatic breakdown[5,6] viscous polysaccharide layer that both cross-links and shields the exposed fibrils addresses that requirement directly.

The results for the laser-only groups present a more complex picture. Standalone conditioning with the 750 nm femtosecond laser showed a high phosphorus recovery, reaching 32,880.58 a.u. (95.44% retention), outperforming the combined groups on this specific element. A plausible mechanism is that sub-ablation near-infrared irradiation at parameters below the reported single-shot ablation threshold can modify superficial organic components and increase surface porosity without producing thermal destruction, consistent with the observation that dentine ablation thresholds are lower than those of enamel and that operation below threshold produces minimal thermal load and no collateral damage[10]. The safe nature of this structural modification is supported by the significant post-treatment microhardness increase observed in Group 1 relative to its carious floor ($p < 0.001$), which validates that sub-threshold near-infrared conditioning does not destroy the tissue. A further contributor may be the wavelength dependence of tissue interaction: infrared irradiation has the highest single-shot ablation threshold of the wavelengths examined in dental hard tissue ($1.1 \pm 0.1$ J/cm² for enamel and $0.6 \pm 0.1$ J/cm² for dentine), whereas shorter wavelengths ablate more efficiently but deliver higher photon energy and therefore greater potential for damage[9]. At the sub-ablation fluencies used here, this infrared regime favors surface modification over material removal.

On the other hand, the standalone 830 nm laser was less effective, with calcium intensity limited to 50,765.68 a.u. The combination of a 750 nm laser and chitosan produced the highest calcium

recovery (56,335.85 a.u.) and strongest surface microhardness. In contrast, phosphorus recovery was relatively suppressed in the combined 830 nm laser-chitosan group (Group 4: 26,829.37 a.u.). This opposes the linear synergy claims documented in various conventional dental laser investigations and contests a simple additive impact, suggesting that near-infrared laser wavelengths create separate absorption kinetics in interplay with a biopolymer hydrogel[38]. These non-linear patterns of energy deposition indicate that certain photon-polymer crosslinking thresholds control element-specific ion mobilization throughout the interfaced dentinal surface[39].

The fact that superior calcium recovery and surface microhardness are combined with moderate phosphorus recovery in the laser-activated combination groups questions the classical approach of perfect coupling of Ca and P precipitation. There is evidence that remineralization may occur in non-stoichiometric stages. Biomimetic agents promote these non-stoichiometric pathways by creating ion activity gradients at the tissue interface instead of approaching a strict stoichiometry[36]. This has been facilitated by the use of polysaccharide- and peptide-stabilized systems that form variable gradients[40] and biomimetic agarose-chitosan hydrogels that form enamel-like structures[35]. Additional amelogenin-chitosan structures temporarily stabilize amorphous Ca–P clusters into structural linear chains, optimizing the density of the interface and mechanical properties[41].

The photo-physical processes induced by the sub-ablation 750 nm lasers increase the permeability of the matrix, propelling further penetration of the 2% chitosan gel. This reaction reveals a high concentration of amine and carboxyl groups that readily bind divalent calcium ions. Although this intensive chelation is the reason behind the high microhardness (32.34 ± 2.60 VHN) observed in Group 3, the positive surface charge and steric hindrance are localized to cause a temporary saturation imbalance, which kinetically slows the integration of incoming phosphate networks into a mature crystal lattice. This non-thermal surface activation is in sharp contrast to threshold or near-threshold dental laser regimes, like femtosecond micro -cavity melting architectures[42], or Nd:YAG systems, which cause immediate stoichiometric precipitation of minerals or crystalline phase changes in tissue through structural melting, recrystallization, and collagen degradation[43]. Consequently, sub-threshold parameters act through safe physical infiltration of the biopolymer without thermal tissue alterations[42].

**Clinical Implications and Future Perspectives**

- This study offers a promising, non-thermal chairside workflow for advanced minimal intervention operative dentistry, especially when treating compromised deep carious lesions.

The clinical importance of this protocol can be summarized in three main values:

- Patient Comfort and Acceptance: Operating at a gentle sub-ablation threshold of 300 mW, the near-infrared femtosecond laser serves as a safe alternative to conventional rotary instruments, completely eliminating handpiece noise, friction, vibrations, and intrapulpal thermal stress.
- Scaffold Stabilization and MMP Inhibition: The photo-physical matrix activation successfully unroofs blocked dentinal tubules and increases surface free energy without

causing micro-cracking or collagen denaturation, driven by deep tubular infiltration of the concentrated 2% chitosan gel which structurally cross-links the organic scaffold and actively inhibits MMPs.

- Enhanced Restoration Longevity: By achieving a post-treatment surface microhardness peak of 32.34 ± 2.60 VHN within the 750 nm cohort and stabilizing native phosphorus element networks, this combined technique successfully reinforces compromised dental matrices, preserves vital pulp tissue, and extends the long-term clinical lifespan of adhesive resin restorations against progressive erosive mineral dissolution over time.

**Study Limitations**

- In vitro design: This short-term in vitro protocol is not able to simulate the dynamic aspects of oral complexity such as the continuous salivary flow, the variation in pH, and active biofilm challenges.
- Restricted Parameter Scope: It was only tested with two near-infrared profiles and a certain 2% medium molecular weight physical hydrogel. A change in the laser parameters or the concentration of the biopolymer might result in completely different infiltration and chelation kinetics.
- Immediate Dry Evaluation: The samples were analysed in a strictly dry laboratory setting right after the treatment to prevent external ion contamination from skewing the LIBS results. Although this dry isolation was necessary to the spectral accuracy, it does not allow tracing of long-term cyclic fatigue or dynamic enzymatic resistance.
- **Conclusion**
- Joint use of a 750 nm near-infrared femtosecond laser and 2% chitosan hydrogel is a safe, effective and non-destructive biomodification paradigm of deep carious dentine.
- This synergistic configuration significantly improves substrate surface microhardness, statistically outperforming standalone laser modalities.
- Sub-ablation 750 nm laser activation optimizes localized calcium mineral intensity recovery, successfully returning the carious matrix close to its baseline parameters.
- Standalone topical delivery of 2% chitosan gel shows distinct chemical shielding mechanisms that provide effective mechanical stabilization after demineralization and maintain post-treatment Phosphorus network retention at 79.41%.
- Calcium and phosphorus follow independent, decoupled kinetic pathways during treatment, so that this combined, non-thermal protocol is a highly promising, minimally invasive clinical method to strengthen weakened dental matrices.

**Acknowledgements**

Not applicable.

## Author Contributions

The study was conceptualized by M. G. M., S. H. E., A. E., F. A., W. A., M. N., and T.M. Data were curated by M. G. M. and A. E. Investigation and methodology were carried out by M. G. M., S. H. E., A. E., F. A., W. A., M. N., and T.M. Software support and formal analysis were provided by M. G. M. and S. H. E. Supervision was undertaken by W. A., M. N., and T.M. Validation and visualization were performed by M. G. M. and A. E. The initial draft was prepared by M. G. M., F. A., and A. E., while all authors participated in reviewing and editing the manuscript. All authors approved the final version for publication.

## Funding

The authors declare that no funds, grants, or other financial support were received from any public, commercial, or non-profit funding agencies during the preparation of this manuscript.

## Data Availability Statement

The raw and processed datasets generated and analyzed during the current investigation are not publicly deposited due to institutional privacy protocols, but they are fully available from the corresponding author upon reasonable academic request.

## Consent for Publication

Not applicable.

## Ethics Declarations

## Ethics Approval and Consent to Participate

This study protocol was officially reviewed and approved by the Research Ethics Committee of the Faculty of Dentistry, Minia University (Approval No. 690/2023). All experimental procedures and human tissue handling methodologies were executed in strict accordance with the ethical principles, guidelines, and regulations outlined in the World Medical Association Declaration of Helsinki. Written informed consent was voluntarily obtained from all human donors prior to tooth extraction, which included comprehensive disclosures regarding the specific research objectives and the ultimate deployment of the extracted waste specimens for *in vitro* laboratory analysis.

## Competing Interests

The authors declare that they have no known competing financial interests, personal relationships, or professional conflicts of interest that could have appeared to influence the work reported in this paper.

## References


1. Mokeem LS, Garcia IM, Melo MA. Degradation and failure phenomena at the dentin bonding interface. Biomedicines. 2023;11(5):1256.

2. Pashley DH, Tay FR, Yiu C, Hashimoto M, Breschi L, Carvalho RM, et al. Collagen Degradation by Host-derived Enzymes during Aging. J Dent Res. 2004 Mar;83(3):216–21. doi:10.1177/154405910408300306

3. Tay FR, Pashley DH, Su BI, Hiraishi N, Yiu CKY. Water treeing in simplified dentin adhesives-deja vu? OPERATIVE DENTISTRY-UNIVERSITY OF WASHINGTON-. 2005;30(5):561.

4. Tay FR, Hashimoto M, Pashley DH, Peters MC, Lai SCN, Yiu CKY, et al. Aging Affects Two Modes of Nanoleakage Expression in Bonded Dentin. J Dent Res. 2003 Jul;82(7):537–41. doi:10.1177/154405910308200710

5. Montagner AF, Sarkis-Onofre R, Pereira-Cenci T, Cenci MS. MMP Inhibitors on Dentin Stability: A Systematic Review and Meta-analysis. J Dent Res. 2014 Aug;93(8):733–43. doi:10.1177/0022034514538046

6. Tjäderhane L, Nascimento FD, Breschi L, Mazzoni A, Tersariol IL, Geraldeli S, et al. Strategies to prevent hydrolytic degradation of the hybrid layer—a review. Dental materials. 2013;29(10):999–1011.

7. Frencken JE, Peters MC, Manton DJ, Leal SC, Gordan VV, Eden E. Minimal intervention dentistry for managing dental caries – a review. International Dental Journal. 2012 Oct;62(5):223–43. doi:10.1111/idj.12007

8. de Moura RC, Santos PS, dos Santos Matias PM, Vitali FC, Hilgert LA, Cardoso M, et al. Knowledge, attitudes, and practice of dentists on Minimal Intervention Dentistry: A systematic review and meta-analysis. Journal of Dentistry. 2023;132:104484.

9. Rapp L, Madden S, Brand J, Maximova K, Walsh LJ, Spallek H, et al. Investigation of laser wavelength effect on the ablation of enamel and dentin using femtosecond laser pulses. Sci Rep. 2023 Nov 17;13(1):20156. doi:10.1038/s41598-023-47551-5

10. Petrov T, Pecheva E, Walmsley AD, Dimov S. Femtosecond laser ablation of dentin and enamel for fast and more precise dental cavity preparation. Materials Science and Engineering: C. 2018;90:433–8.

11. Lagunov VL, Walsh LJ, Ali B, Rybachuk M, George R. Assessment of dose-dependent surface modification of human enamel and dentin with ultrashort femtosecond 30-fs 800 nm laser irradiation. Optics & Laser Technology. 2025;181:111993.

12. AboElhassan RG, Eltaweel AM. Impact of laser-assisted and different pre-treatment modalities on dentin surface interface and bond strength of fiber posts (In-vitro study). Head & Face Medicine. 2026 Jun 22. doi:10.1186/s13005-026-00632-y

13. Berradi A, Aziz F, Achaby ME, Ouazzani N, Mandi L. A Comprehensive Review of Polysaccharide-Based Hydrogels as Promising Biomaterials. Polymers. 2023 Jul;15(13):2908. doi:10.3390/polym15132908

14. Qu S, Ma X, Yu S, Wang R. Chitosan as a biomaterial for the prevention and treatment of dental caries: antibacterial effect, biomimetic mineralization, and drug delivery. Front Bioeng Biotechnol. 2023 Sep 29;11:1234758. doi:10.3389/fbioe.2023.1234758

15. Cai J, Moradian-Oldak J. Triple Function of Amelogenin Peptide-Chitosan Hydrogel for Dentin Repair. J Dent Res. 2023 Dec;102(13):1434–43. doi:10.1177/00220345231198228

16. Ren Q, Ding L, Li Z, Wang X, Wang K, Han S, et al. Chitosan hydrogel containing amelogenin-derived peptide: Inhibition of cariogenic bacteria and promotion of remineralization of initial caries lesions. Archives of oral biology. 2019;100:42–8.

17. Özcan M, Barbosa SH, Melo RM, Galhano GA, Bottino MA. Effect of surface conditioning methods on the microtensile bond strength of resin cement to deep dentin. J Biomed Mater Res B Appl Biomater. 2012;100(1):202–8.

18. Marquezan M, Corrêa FNP, Sanabe ME, Rodrigues Filho LE, Hebling J, Guedes-Pinto AC, et al. Artificial methods of dentine caries induction: A hardness and morphological comparative study. Archives of oral biology. 2009;54(12):1111–7.

19. François P, Benoit A, Slimani L, Dufresne A, Gouze H, Attal JP, et al. In vitro remineralization by various ion-releasing materials of artificially demineralized dentin: A micro-CT study. Dental Materials. 2024;40(3):520–6.

20. Serbanoiu DC, Vartolomei AC, Ghiga DV, Pop SI, Panainte I, Moldovan M, et al. Comparative evaluation of dental enamel microhardness following various methods of interproximal reduction: A Vickers hardness tester investigation. Biomedicines. 2024;12(5):1132.

21. Küçükkaya Eren S, Uzunoğlu-Özyürek E, Sezer B, Yilmaz Z, Boyacı I. Mineral content analysis of root canal dentin using laser-induced breakdown spectroscopy. Restorative Dentistry & Endodontics. 2018 Feb 4;43. doi:10.5395/rde.2018.43.e11

22. Roberts WE, Mangum JE, Schneider PM. Pathophysiology of Demineralization, Part I: Attrition, Erosion, Abfraction, and Noncarious Cervical Lesions. Curr Osteoporos Rep. 2022;20(1):90–105. doi:10.1007/s11914-022-00722-1 PubMed PMID: 35129809; PubMed Central PMCID: PMC8930910.

23. Pashley DH, Tay FR, Breschi L, Tjäderhane L, Carvalho RM, Carrilho M, et al. State of the art etch-and-rinse adhesives. Dental Materials. 2011 Jan;27(1):1–16. doi:10.1016/j.dental.2010.10.016

24. Baena E, Cunha SR, Maravić T, Comba A, Paganelli F, Alessandri-Bonetti G, et al. Effect of Chitosan as a Cross-Linker on Matrix Metalloproteinase Activity and Bond Stability with Different Adhesive Systems. Mar Drugs. 2020 May 18;18(5):263. doi:10.3390/md18050263 PubMed PMID: 32443628; PubMed Central PMCID: PMC7280998.

25. Šalinović I, Bilić-Prcić M, Bota M, Ivica A, Miletić I. Microhardness Recovery and Micromorphology of Demineralized Dentin Restored with Modified Glass Hybrid Material. Materials (Basel). 2026 Apr

24;19(9):1733. doi:10.3390/ma19091733 PubMed PMID: 42124140; PubMed Central PMCID: PMC13165214.

26. Samek O, Telle HH, Beddows DC. Laser-induced breakdown spectroscopy: a tool for real-time, in vitro and in vivo identification of carious teeth. Vol. 1. 2001 Dec 19;1:1. doi:10.1186/1472-6831-1-1 PubMed PMID: 11801201; PubMed Central PMCID: PMC64785.

27. Gazmeh M, Bahreini M, Tavassoli SH. Discrimination of healthy and carious teeth using laser-induced breakdown spectroscopy and partial least square discriminant analysis. Appl Opt. 2015 Jan 1;54(1):123. doi:10.1364/AO.54.000123

28. Ahmed E, Mohamed T, Kandil H. Monitoring Elemental Changes in Human Teeth with Laser-Induced Breakdown Spectroscopy: Novel Approaches and Experimental Understandings. Laser Innovations for Research and Applications. 2026 Jun 1. doi:10.21608/lira.2026.492026.1036

29. Mustafa M, Latif A, Jehangir M. Laser-Induced Breakdown Spectroscopy and Microscopy Study of Human Dental Tissues. In: Electron Microscopy. IntechOpen; 2022. doi:10.5772

30. Tareq MS, Hamad TK. Heavy metal migration from dental filling materials to calcified oral tissues: an in vitro analysis using LIBS and ICP-MS techniques. Odontology. 2025 Oct 1;113(4):1613–23. doi:10.1007/s10266-025-01088-3

31. Pořízka P, Konečná A, Šindelářová A, Šulcová M, Modlitbová P, Prochazka D, et al. Feasibility of laser-induced breakdown spectroscopy to elucidate elemental changes in human tooth ankylosis. Spectrochimica Acta Part B: Atomic Spectroscopy. 2023 Aug 1;206:106727. doi:10.1016/j.sab.2023.106727

32. Motto-Ros V, Gardette V, Sancey L, Leprince M, Genty D, Roux S, et al. LIBS-Based Imaging: Recent Advances and Future Directions. Journal of Spectroscopy [Internet]. 2020 Feb [cited 2026 Sep 22];35(2):34–40. Available from: https://hal.science/hal-02998713

33. Li S, Teng F, Ren L, Yan Q, Ye W, Tian Y, et al. Long-pulsed laser-induced breakdown spectroscopy for elemental imaging: An evaluation with human teeth. Spectrochimica Acta Part B: Atomic Spectroscopy. 2025 Jul 1;229:107201. doi:10.1016/j.sab.2025.107201

34. de Freitas PM, Soares-Geraldo D, Biella-Silva AC, Silva AV, da Silveira BL, Eduardo C de P. INTRAPUPAL TEMPERATURE VARIATION DURING ER,CR:YSGG ENAMEL IRRADIATION ON CARIES PREVENTION. J Appl Oral Sci. 2008 Apr;16(2):95–9. doi:10.1590/S1678-77572008000200003 PubMed PMID: 19089198; PubMed Central PMCID: PMC4327626.

35. Muşat V, Anghel EM, Zaharia A, Atkinson I, Mocioiu OC, Buşilă M, et al. A Chitosan–Agarose Polysaccharide-Based Hydrogel for Biomimetic Remineralization of Dental Enamel. Biomolecules. 2021 Aug 2;11(8):1137. doi:10.3390/biom11081137

36. Mukherjee K, Chakraborty A, Sandhu G, Naim S, Bauza Nowotny E, Moradian-Oldak J. Amelogenin Peptide-Chitosan Hydrogel for Biomimetic Enamel Regrowth. Front Dent Med. 2021 Jun 16;2. doi:10.3389/fdmed.2021.697544

37. Ren Q, Li Z, Ding L, Wang X, Niu Y, Qin X, et al. Anti-biofilm and remineralization effects of chitosan hydrogel containing amelogenin-derived peptide on initial caries lesions. Regenerative Biomaterials. 2018 Mar 1;5(2):69–76. doi:10.1093/rb/rby005

38. Ma J, Wu J, Lin Z, Wang J, Yao W, Zhang Y, et al. Femtosecond-Laser Preparation of Hydrogel with Micro/Nano-Structures and their Biomedical Applications. Small Sci. 2025 Apr;5(4):2400400. doi:10.1002/smsc.202400400 PubMed PMID: 40657187; PubMed Central PMCID: PMC12244510.

39. Alkhudhairy F. Experimental and Chitosan-Infused Adhesive with Dentin Pretreated with Femtosecond Laser, Methylene Blue-Activated Low-Level Laser, and Phosphoric Acid. Photobiomodul Photomed Laser Surg. 2024 Oct;42(10):634–42. doi:10.1089/pho.2024.0077 PubMed PMID: 39069884.

40. Cochrane NJ, Reynolds EC. Calcium phosphate gradients and interface ion activity under polysaccharide-stabilized dental remineralization models. J Dent Res. 2008;87(11):1052.

41. Ruan Q, Zhang Y, Nutt S, Moradian-Oldak A. An amelogenin-chitosan matrix promotes assembly of an enamel-like layer on etched human enamel. Acta Biomater. 2013;9(7):7289–7297. doi:10.1016/j.actbio.2013.03.023.

42. Javed F, Akhter R, Miletic V. Effects of femtosecond laser on hard dental tissues: A scoping review. Lasers Med Sci. 2024 Nov 20;39(1):286. doi:10.1007/s10103-024-04225-6

43. Pereira DL, Freitas AZ, Bachmann L, Benetti C, Zezell DM, Ana PA. Variation on Molecular Structure, Crystallinity, and Optical Properties of Dentin Due to Nd:YAG Laser and Fluoride Aimed at Tooth Erosion Prevention. Int J Mol Sci. 2018 Feb 1;19(2):433. doi:10.3390/ijms19020433 PubMed PMID: 29389868; PubMed Central PMCID: PMC5855655.

## Supplementary Files

This is a list of supplementary files associated with this preprint. Click to download.

- Graphs.xlsx